Journal of Inclusion Phenomena **6** (1988), 307–318.

Calorimetric Study on Pure and KOH-doped Argon Clathrate Hydrates*

O. YAMAMURO, M. OGUNI, T. MATSUO, and H. SUGA**
Department of Chemistry and Chemical Thermodynamics Laboratory, Faculty of Science, Osaka University, Toyonaka, Osaka 560, Japan

(Received: 20 August 1987; In final form: 15 February 1988)

Abstract. Pure and KOH ($x = 1.3 \times 10^{-3}$)-doped argon clathrate hydrates were synthesized in an adiabatic high-pressure calorimetric cell from one mole of water and 200 MPa of Ar gas. The heat capacities of the hydrates were measured from 12 to 130 K. No anomaly was found in the pure sample but a glass transition considered to be related to a proton-configurational mode of the host hydrogen-bonded lattice was observed for the first time at 55 K in the doped sample. Comparison with the results on pure and KOH-doped tetrahydrofuran clathrate hydrates indicated that the thermodynamic properties of a hydrogen-bonded system depend on the kind of guest molecule. The heat capacity of argon in the hydrate cages was adequately analyzed with the one-dimensional Pöschl-Teller potential as used in the Ar-β-quinol clathrate and the additivity of heat capacities of the guest and host was shown to be valid in the temperature range 12–130 K.

Key words. Calorimetry, argon clathrate hydrate.

1. Introduction

Argon hydrate is the most fundamental clathrate hydrate in the sense that argon is spherical and the smallest of the molecules which can be accommodated in the clathrate cages and so its interaction with the lattice is the weakest. On the other hand, however, it is the most difficult hydrate to synthesize because of the requirement of high pressure and low temperature conditions. The crystal structure of the Ar-hydrate was recently found to belong to the structure II type by Davidson *et al.* [1]. A unit cell of the structure II type has sixteen 12-hedral and eight 16-hedral cages made up of 136 water molecules [2, 3]. Argon can be enclathrated in both cages so that the ideal composition for the full occupation is $Ar{\cdot}5.67\ H_2O$. The p–T phase diagram of the H_2O–Ar system was determined by Barrer and Edge [4], and Marshall *et al.* [5]. The dielectric properties of the hydrate was studied by Gough *et al.* [6]. However, the thermal properties of the Ar-hydrate have not been studied so far because of the extreme difficulty of complete formation of the hydrate sample, which is quite important for the quantitative calorimetric study.

In this study we prepared the Ar-hydrate crystal inside the cell of the high-pressure calorimeter [7] from one mole of water and Ar gas at 200 MPa. The heat capacities of the pure and KOH-doped samples were measured in the temperature range between 13 and 130 K. This study was focused on the following two important general aspects of clathrate hydrates:

The first is the dynamical and ordering properties of protons in the host lattice. In clathrate hydrates, each water molecule is hydrogen-bonded to four nearest neighbors and

* Contribution No. 128 from Chemical Thermodynamics Laboratory.
** Author for correspondence.

the protons are disordered between two distinct positions on the bonds. But the corresponding proton-ordering transition has not been observed in any hydrate. This situation is the same as in pure ices Ih, Ic, V, and VI [8]. Very recently our calorimetric studies [9–11] showed a glass transition ($T_g = 85$ K, $\Delta C_p = 1.1$ J K^{-1} (H_2O-mol)$^{-1}$) and a first-order phase transition ($T_{trs} = 62$ K, $\Delta_{trs}S = 2.4$ J K^{-1}(H_2O-mol)$^{-1}$) in pure and KOH ($x = 1.8 \times 10^{-4}$, where x is mole fraction of KOH in H_2O and KOH)-doped tetrahydrofuran (THF) clathrate hydrates, respectively. From the consistency with the dielectric data [12], the glass transition was revealed to be a freezing of the configurational motion of protons disordered in the host lattice. The mechanism of the phase transition is not completely clarified, but it is considered to be related to a proton-ordering, as judged from the large entropy change and also from the fact that the transition was induced by doping with KOH as in the case of KOH-doped hexagonal ice [13, 14]. In ices [14–15], it is known that KOH incorporated into the lattice produces L orientational defects and enhances the configurational motion of protons. In the Ar-hydrate, the glass transition is expected to take place at 90–100 K by extrapolating the dielectric relaxation times to the low frequency region (10^3–10^4 s). From the fact that the excess heat capacity due to the short-range ordering of protons still exists at 100 K (ca. 0.6 J K^{-1} (H_2O-mol)$^{-1}$) in the THF-hydrate [11] of the same structure II, a glass transition is expected to occur in the Ar-hydrate if the hydrogen-bonded system is not affected by the guest molecules. For the KOH-doped Ar-hydrate, it is unknown whether KOH dissolves in the hydrate crystal and does not affect the equilibrium thermodynamic properties of the hydrate. However if any KOH-effect on the ordering of protons is observed in the most simple Ar-hydrate, it would give important information for understanding the nature of the transition found in the KOH-doped THF-hydrate.

The second interest of this study is the motion of argon in the hydrate cage and the additivity of heat capacities of the guest and host. In Ar-β-quinol clathrate, whose cage has almost the same size as the 12-hedral cage of the clathrate hydrate (ca. 800 pm), Parsonage and Staveley [16] showed that the heat capacity is a linear function of the occupancy of argon down to 20 K; i.e., the additivity of heat capacities of the guest and host is valid. Hence the heat capacity of the empty lattice could be obtained by extrapolating the experimental heat capacities to zero occupancy. In the clathrate hydrate of Xe and Kr, calorimetric [17] and theoretical [18] studies by Handa *et al.* indicated that such additivity is equally valid and also the heat capacity of the empty host lattice can be expressed by that of hexagonal ice, at least down to 80 K. However at low temperature and for the Ar-hydrate, no information has been obtained so far.

2. Experimental

Water was purified by distillation followed by deionization, and its conductance was less than 0.1 μS cm^{-1}. The purity of Ar gas (Seitetsu Kagaku Ind., Co. Ltd.) was claimed to be more than 99.999%. The KOH-doped aqueous solution was prepared by mixing KOH (0.1 mol dm^{-3}) solution for volumetric analysis (Wako Pure Chemical Ind., Ltd.) with the purified water. Its concentration was 1.3×10^{-3} in the mole fraction of KOH. The masses of water used for the synthesis and the subsequent heat capacity measurement were 17.847 g for the pure sample and 18.213 g for the KOH-doped sample, each corresponding to 0.99066 mol and 1.0110 mol.

Figure 1 shows the p–T phase diagram of the Ar–H_2O system. The hydrate is stable in the low temperature and high pressure region (unshaded area in the figure). Dotted lines

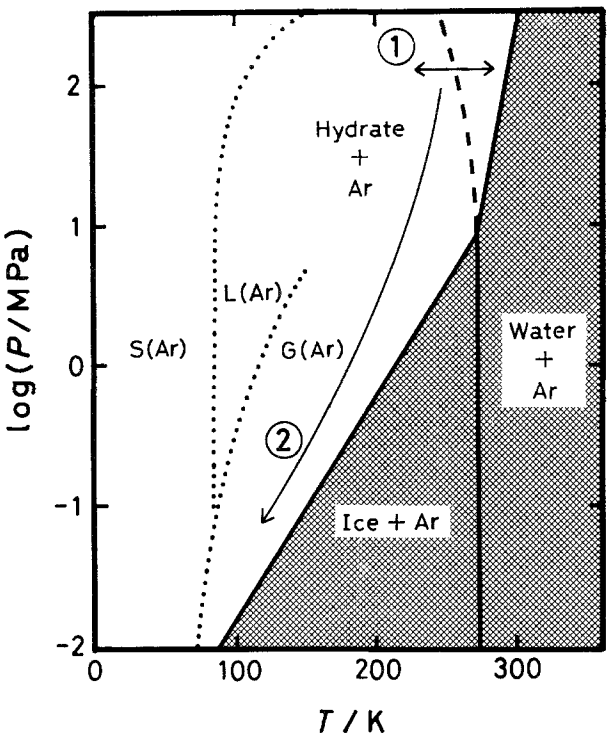

Fig. 1. p–T phase diagram of the Ar–H_2O system [4, 5]. The hydrate is stable in the unshaded region. The dashed line represents the melting line of ice in the metastable state. Dotted lines represent the phase boundaries among the three states of aggregation of pure Ar [19]. The hydrate was prepared by following the route shown by arrows (①, ②).

represent the boundaries among the three states of aggregation of pure Ar [19]. In the present study, the Ar-hydrate was synthesized inside the cell of the high pressure calorimeter [7] from water and 200 MPa of Ar gas at around 250 K. Argon was supplied continuously during the synthesis through the tube connected to the cell from the high pressure system of the calorimeter. It was found that the formation of the hydrate was accelerated by repeated crystallization and melting of water (ca. 255 K) as indicated by ① in Fig. 1. Since the solubility of Ar in water is very low even at high pressure, the reaction takes place mainly at the interface between water and Ar gas, resulting in the partitioning between both reactants by the hydrate crystal formed and thus the rapid decrease in the rate of reaction. It is considered that the crystallization of water breaks the shell of the hydrate and creates new interfaces. The extent of reaction could be checked by measuring the enthalpy of fusion of the remaining ice. After the above operation was repeated once a day for about 50 days, the temperature and pressure of the sample were decreased through the path ② in order to avoid both decomposition of the hydrate and solidification of Ar gas. The final degree of the reaction was 99.7% in H_2O for the pure sample.

The occupancy of argon in the hydrate was not checked directly but can be checked by using the ideal solution theory developed by van der Waals [20]. The occupancy of argon is expressed by the equation:

$$\phi = \frac{Kf}{1 + Kf}. \tag{1}$$

Here, K is the Langmuir equilibrium constant, and f is the fugacity of argon. The constant K for the 12-hedral cage has been estimated to be 3×10^{-6} Pa^{-1} at 250 K from the measurement on the mixed hydrate with chloroform [4]. Assuming that the fugacity is equal to the pressure and the value of K for the 16-hedral cage is the same as that for the 12-hedral cage and does not change even at 200 MPa, ϕ at 200 MPa and 250 K is calculated to be 0.998. This guarantees that the composition of the hydrate formed in this study is very close to the ideal Ar·5.67 H_2O. The following heat capacity data and analysis are based on this composition.

For the KOH-doped sample, however, the formation of the hydrate was incomplete and unfortunately excess Ar gas was occluded in the space among the hydrate crystals (not in the hydrate cages), so that the absolute heat capacity values of the hydrate could not be obtained. This is an unwelcome effect of KOH and is now under investigation.

According to Fig. 1, the vapor pressure curve of solid Ar will intersect the dissociation pressure curve of the hydrate around 80 K and so the vapor pressure of Ar is lower than the dissociation pressure of the hydrate below 80 K. This means that pure Ar is more stable than the hydrate below 80 K. Actually, however, the dissociation did not take place probably for kinetic reasons. This was confirmed by the fact that the heat capacity of the hydrate did not change through several cycles of measurement between 12 and 130 K.

Heat capacity measurements were performed with the adiabatic high-pressure calorimeter [7] in the temperature range of 13 to 130 K. Helium gas at 0.01 MPa and Ar gas at 0.1 MPa were charged in the cell in the ranges 13–90 K and 90–130 K, respectively. They served to suppress the decomposition of the hydrate and to facilitate thermal contact between the sample and the cell. The precision of the heat capacity measurement was within 0.1% above 30 K.

3. Results and Discussion

3.1. HEAT CAPACITY OF THE PURE Ar-HYDRATE

Experimental heat capacities and the thermodynamic functions derived from them are tabulated in Tables I and II, respectively. The heat capacity below 13 K was estimated by the following extrapolation: only the lattice vibration of the host lattice (5.67×3 degrees of freedom) and the translational vibration of argon in the cage (3 degrees of freedom) contribute effectively to the heat capacity in this temperature range. The former contribution was approximated by the 2 Debye functions, each having 5.67×1 and 5.67×2 degrees of freedom, respectively, and the latter was by the Einstein function having 3 degrees of freedom. The parameters of the functions [$\theta_D(5.67)$, $\theta_D(11.34)$, $\theta_E(3)$; numbers in parentheses represent the degrees of freedom] were determined by least squares fitting so as to reproduce the experimental data below 30 K. The following set of parameters was obtained; $\theta_D(5.67)/K = 148.6$, $\theta_D(11.34)/K = 427.5$, and $\theta_E(3)/K = 34.59$.

Figure 2 shows the heat capacities listed in Table I as quantities per mole of H_2O. The lower line represents the molar heat capacity of ice Ih, so the difference between both the curves gives the contribution from argon enclathrated in the hydrate cages. This will be discussed in detail in section 3.3. Figure 3 shows the encraty (C_p/T) and the corresponding temperature drift rates observed 20 min after each heating period in the temperature range 80–130 K. From the extrapolation of the dielectric relaxation time [6], a glass transition due to the proton configurational motion was expected to occur at 90–100 K. However, any systematic temperature drift characteristic of the glass transition was not observed

Table I. Molar heat capacities of Ar·5.67 H_2O.

T_{av}/K	$C_{p,m}$/J K^{-1} mol^{-1}	T_{av}/K	$C_{p,m}$/J K^{-1} mol^{-1}	T_{av}/K	$C_{p,m}$/J K^{-1} mol^{-1}	T_{av}/K	$C_{p,m}$/J K^{-1} mol^{-1}
13.47	17.77	34.53	48.24	64.81	79.84	95.70	106.1
14.29	19.19	35.93	49.93	66.37	81.34	97.31	107.3
15.37	20.91	37.33	51.57	67.95	82.79	98.93	108.6
16.10	22.03	38.72	53.17	69.54	84.29	100.58	109.9
16.76	23.08	40.12	54.74	71.13	85.72	102.24	111.2
17.38	24.04	41.51	56.29	72.73	87.04	103.92	112.5
17.95	24.93	42.90	57.81	74.31	88.44	105.62	113.7
18.52	25.79	44.28	59.30	75.88	89.87	107.34	115.0
19.10	26.73	45.66	60.79	77.44	91.27	109.08	116.2
19.70	27.62	47.03	62.28	78.99	92.66	110.83	117.5
20.52	28.94	48.42	63.68	80.68	94.14	112.60	118.7
21.59	30.53	49.84	65.15	82.10	95.26	114.39	120.0
22.74	32.26	51.27	66.76	83.53	96.45	116.19	121.3
23.94	34.05	52.72	68.21	84.98	97.71	118.02	122.6
25.15	35.81	54.18	69.70	86.45	98.86	119.86	124.0
26.41	27.59	55.66	71.13	87.94	100.1	121.72	125.3
27.73	39.40	57.16	72.58	89.46	101.3	123.59	126.5
29.07	41.18	58.66	74.04	90.99	102.6	125.49	127.7
30.42	42.98	60.18	75.54	92.54	103.7	127.40	129.1
31.77	44.75	61.71	76.96	94.11	104.9	129.32	130.6
33.15	46.53	63.26	78.42				

within our thermometry limit ($\sim 100\ \mu$K), and no heat capacity anomaly was found even in the encraty plot. The encraty is a slowly changing function with temperature and makes it easy to see a minor change in heat capacity. Extrapolation of the dielectric relaxation time is considered to be virtually error free, and so these results indicate that the configurational motion of protons in the hydrogen-bonded host lattice is frozen-in before any short-range order develops. In the THF-hydrate, the excess heat capacity corresponding to

Table II. Standard thermodynamic functions of Ar·5.67 H_2O.

T/K	$C^\circ_{p,m}/R$	$[H^\circ_m(T) - H^\circ_m(0)]/RT$	$[S^\circ_m(T) - S^\circ_m(0)]/R$	$-[G^\circ_m(T) - H^\circ_m(0)]/RT$
10	(1.349)*	(0.3735)*	(0.4815)*	(0.1081)*
20	3.381	1.394	2.076	0.6811
30	5.109	2.351	3.781	1.430
40	6.567	3.228	5.456	2.228
50	7.864	4.027	7.063	3.036
60	9.063	4.768	8.604	3.836
70	10.18	5.462	10.09	4.624
80	11.25	6.119	11.52	5.397
90	12.23	6.744	12.90	6.154
100	13.16	7.340	14.23	6.895
110	14.06	7.910	15.53	7.622
120	14.91	8.458	16.79	8.334
130	15.78	8.987	18.02	9.032

* Quantities extrapolated from the data above 13 K (see text for the details).

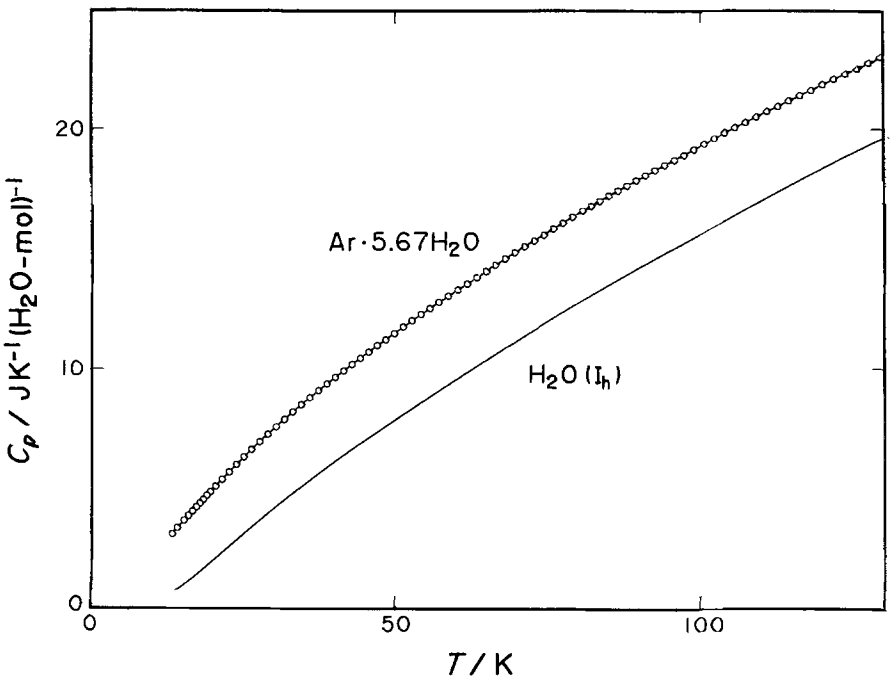

Fig. 2. Heat capacity of Ar·5.67 H_2O represented as the quantity per mole of H_2O. The lower line shows the heat capacity of ice (Ih).

the short-range ordering of protons was still 0.6 J K^{-1} (H_2O-mol)$^{-1}$ at 100 K [10]. Therefore it is clarified that the development of the short-range ordering depends on the kind of guest molecule.

3.2. GLASS TRANSITION IN THE KOH-DOPED Ar-HYDRATE

In the KOH($x = 1.3 \times 10^{-3}$)-doped sample, any phase transition considered to be a proton-ordering was not observed in the whole temperature range 12–130 K but a glass transition was found around 55 K. Figure 4 gives the spontaneous temperature drift rates observed 20 min after each energy supply. In the sample cooled rapidly (0.4 K min^{-1}) (○), an exothermic followed by an endothermic drift appeared in the temperature region 50–70 K. On the other hand, in the sample annealed at 50 K for 18 h (△), only an endothermic drift appeared from 50 K at which the sample was annealed. These dependences of the drift rates on temperature and thermal history of the sample are typical of the glass transition which is essentially the enthalpy relaxation phenomenon from a non-equilibrium to an equilibrium state [21]. Figure 5 shows the corresponding encraty plots, together with the data of the pure Ar-hydrate shown in Fig. 2. Each encraty curve of the doped sample has a jump of about 0.015 J K^{-2} (H_2O-mol)$^{-1}$, which corresponds to a heat capacity jump of 0.9 J K^{-1} (H_2O-mol)$^{-1}$. This glass transition is considered to be related to the proton configurational motion in the host lattice from the fact that it was induced by doping the hydrate with a little amount of KOH. The excess heat capacity above the glass transition temperature was considered to be a tail on the high temperature side of the hypothetical proton-ordering transition, as in the cases of ice Ih [22], ice Ic [15], and THF-hydrate [10].

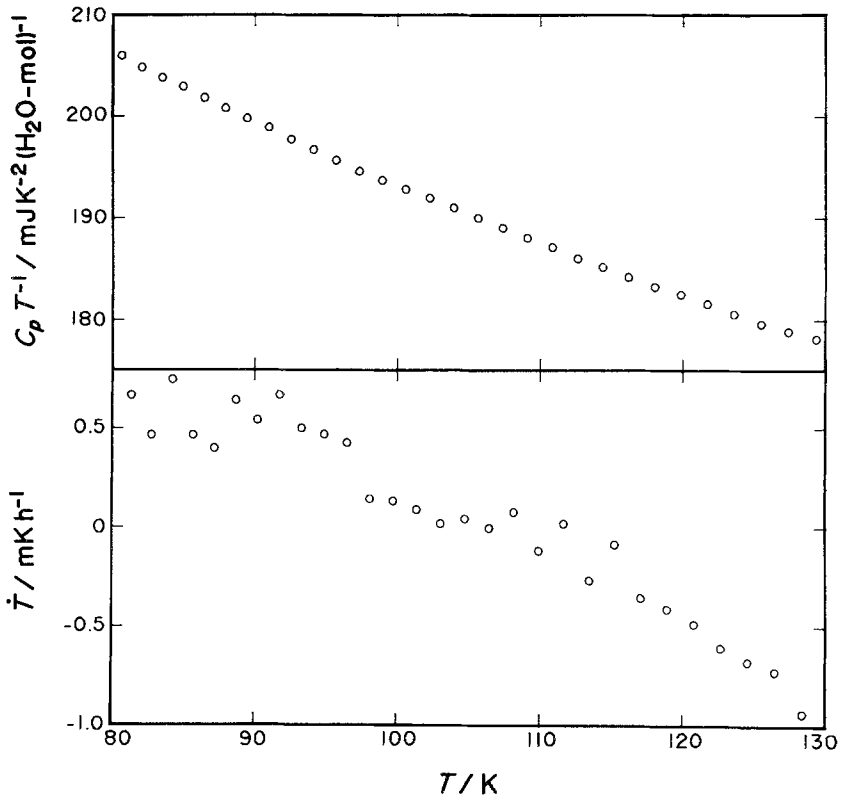

Fig. 3. Encraty (upper) and the corresponding temperature-drift rates (lower) of pure Ar·5.67 H_2O in the temperature range where a glass transition is expected to occur from the dielectric data [6].

KOH dissolved in the hydrate crystal played a catalytic role for the mobility of protons and lowered the proton-freezing down to 55 K. It is significant that the short-range ordering of the protons was found in the simplest clathrate hydrate. However, any transition did not appear at 62 K which is the transition temperature of the THF-hydrate. This indicates that the thermodynamic property governing not only the short-range ordering of the protons, but also the long-range ordering (phase transition) is affected by some properties of the guest molecules.

Two peaks observed at 72 K and 84 K (heat capacity values are located out of the scale of the figure) are clearly ascribed to the proton-ordering transition of the remaining KOH-doped hexagonal ice [13, 14] and melting of Ar [19] occluded in the space among the polycrystals of the hydrate, respectively. Both of them are therefore not the properties of Ar-hydrate itself. The reason why the heat capacity of the doped sample below the glass transition temperature was smaller than that of the pure hydrate is that the former sample had less enclathrated argon than the latter, since the enclathrated argon makes a bigger contribution to the heat capacity than pure crystalline Ar. Furthermore the heat capacity values above 80 K were considered to involve a small contribution from the enthalpy of vaporization of Ar. However the glass transition is considered to be free from the effect of the coexisting impurities (hexagonal ice and Ar). This is because the remaining ice Ih showed the ordering transition at the same temperature as the sole specimen of KOH-doped ice (72 K). The ice part of the sample existed independently of the Ar-hydrate. Solid

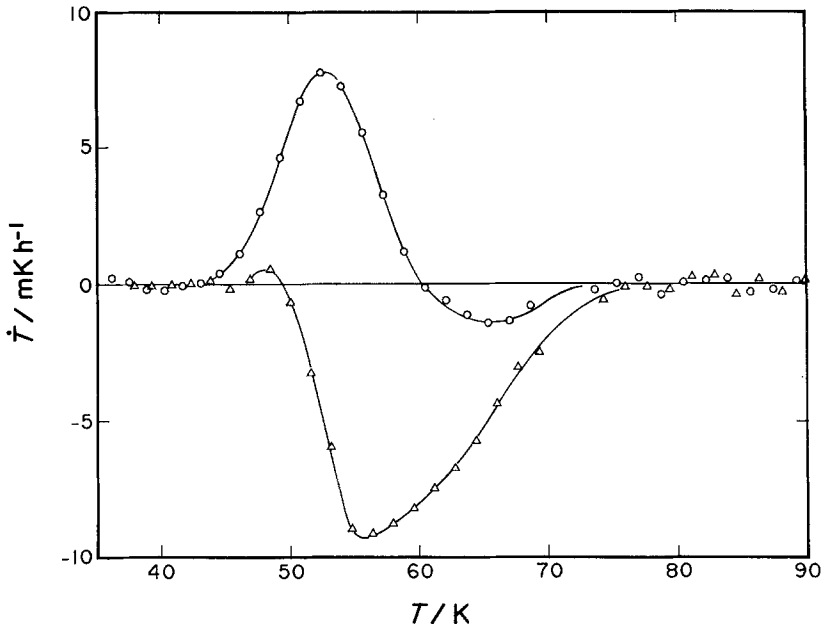

Fig. 4. Spontaneous temperature-drift rates of KOH (1.3×10^{-3})-doped Ar·5.67 H_2O. ○: cooled at 0.4 K min^{-1}, △: annealed at 50 K for 18 h.

Ar is a molecular crystal so that its coexistence has little effect on the properties of the hydrogen-bonded network of the Ar-hydrate. Anyway this unwelcome KOH-effect on the formation of the hydrate mars the accuracy of the heat capacity measurements of the doped sample. A sample with less KOH-concentration should be measured in future in

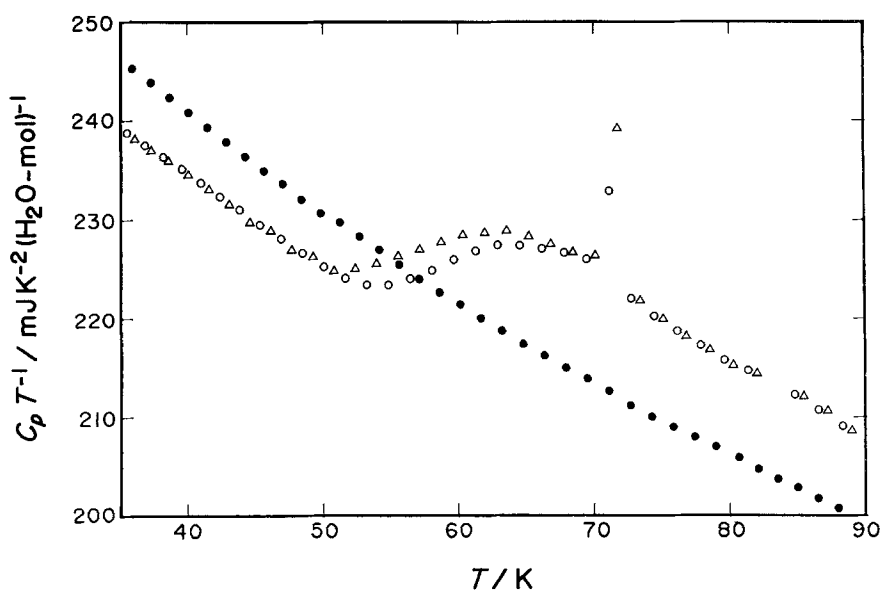

Fig. 5. Encraty plots of KOH (1.3×10^{-3})-doped Ar·5.67 H_2O (○: cooled at 0.4 K min^{-1}, △: annealed at 50 K for 18 h) and pure Ar·5.67 H_2O (●).

order to determine the molar heat capacity of the KOH-doped sample and clarify the KOH-effect further.

3.3. MOTION OF ARGON IN THE HYDRATE CAGES AND COMPARISON WITH THAT FOR Ar-β-QUINOL CLATHRATE

To derive the heat capacity of the encaged argon, the heat capacity of the host lattice was subtracted from the total assuming that it was the same as that of hexagonal ice and the simple additivity of heat capacities of the guest and host is valid. These assumptions have already been confirmed in Kr- and Xe-hydrates in the temperature range above 80 K [17, 18], but in the Ar-hydrate it has not been confirmed so far.

Open circles in Fig. 6 show the molar heat capacities of argon enclathrated in the hydrate cages obtained in the way described above. Those in β-quinol clathrate [16] are also given by closed circles. The cage of the β-quinol clathrate is quite similar to the 12-hedral cage of the hydrate with respect to the average geometrical diameter (780 pm) and the constituent atoms of the cage (oxygen). Both heat capacity curves are almost the same in the high temperature region but argon in the hydrate cage has a larger heat capacity than that in the β-quinol clathrate in the low temperature region. This reason will be discussed later.

The motion of the guest molecule in the clathrate cage, which has an intermediate nature between harmonic vibration and free translation, is called "rattling". Since the hydrate has

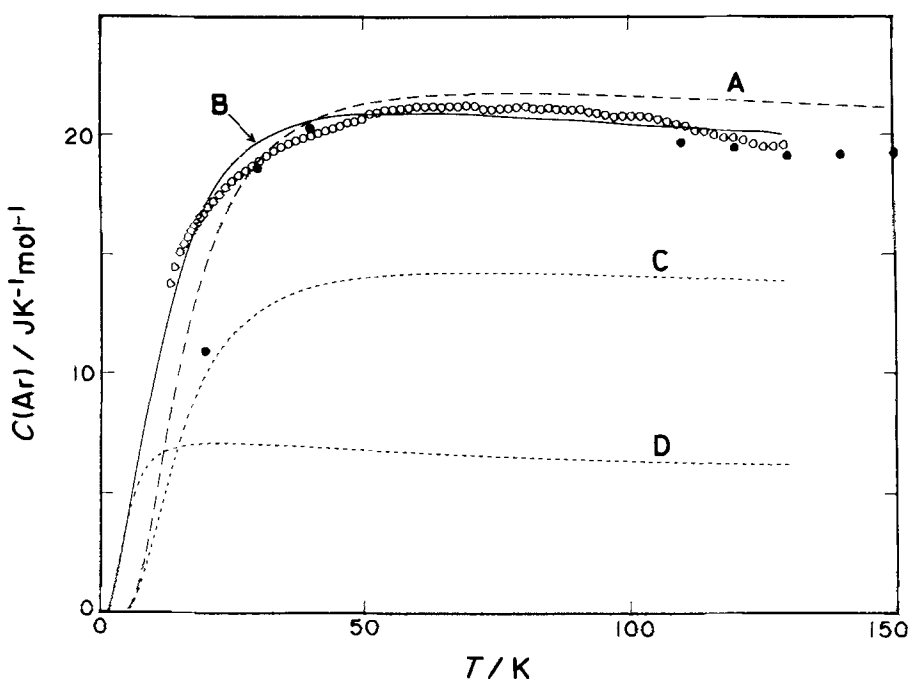

Fig. 6. Molar heat capacities of argon enclathrated in the hydrate cages (○) and the β-quinol clathrate cages (●) [16]. The lines A–D show the heat capacities of argon in the following cages calculated using the Pöschl-Teller potential. A: β-quinol clathrate cages, B: hydrate 12-hedral cages (for 2/3 mol of argon) and 16-hedral cages (1/3), C: hydrate 12-hedral cages (2/3), D: hydrate 16-hedral cages (1/3). Parameters (a and d_0) were obtained from the far-infrared data [24] for A and from the least-squares fitting for B, C, and D.

cubic symmetry, its potential can be described by the one-dimensional Pöschl-Teller potential [23, 24],

$$V(x) = \frac{h^2 a(a-1)}{8md_0^2 \sin^2[(x/d_0) - 1/2]}, \tag{2}$$

where h is Planck's constant, m is the mass of the guest, d_0 is the distance through which the guest can move in the cage, and a is a parameter reflecting the stiffness of the cage, implying that the larger a is the stiffer the cage wall is. The energy levels for this potential are given by

$$E_n = (h^2/8md_0^2)(a+n)^2 \qquad n = 0, 1, 2, \ldots, \tag{3}$$

where n is the quantum number for the rattling motion.

In the Ar-β-quinol clathrate $a = 23.2$ and $d_0 = 236$ pm, which were obtained from the frequencies for the $n = 0 \rightarrow n = 1$ and $n = 1 \rightarrow n = 2$ transitions in far-infrared spectra [24]. The heat capacity calculated from eq. (3) with the parameters $a = 23.2$ and $d_0 = 236$ pm is shown by line A in Fig. 6, reproducing the experimental data reasonably. The structure II clathrate hydrate has sixteen 12-hedral and eight 16-hedral cages per unit cell so that the molar heat capacity of encaged argon is expressed as

$$C(\text{total}) = (1/3)C(16) + (2/3)C(12). \tag{4}$$

The calculation includes four parameters $a(12)$, $a(16)$, $d_0(12)$, $d_0(16)$ to be determined. No far-infrared data on the Ar-hydrate have been obtained and so we tried to determine these parameters with the following method.

First we estimated the values of $d_0(12)$ and $d_0(16)$ to be 170 pm and 330 pm, respectively, by subtracting the hard sphere diameters of argon (340 pm) and oxygen (270 pm) from the respective geometrical cage diameters (780 pm and 840 pm). The diameters of argon and oxygen were estimated as the σ^* values of the Lennard-Jones potential,

$$U(r) = 4\varepsilon[(\sigma^*/r)^{12} - (\sigma^*/r)^6]. \tag{5}$$

This method, and the parameters σ^* used, were the same as those employed by Neece and Poirier [23] in the case of the Ar-β-quinol clathrate. The remaining two parameters $a(12)$ and $a(16)$ were determined by least-squares fitting so as to reproduce the experimental heat capacity of Ar in hydrate cages. The fit was fairly good and the parameters determined were as follows: $a(12) = 10.3$ and $a(16) = 27.9$. These values are comparable in magnitude with the parameter a of the Ar-β-quinol clathrate. However, it is not acceptable physically that $a(16)$ is about three times larger than $a(12)$, since the interacting atoms are the same (argon and oxygen) in both the 12-hedral and 16-hedral cages. By the way, the fitting assuming $a(12) = a(16)$ with these fixed d_0 values could not reproduce the experimental heat capacity at all.

Next, we treated $a(12)$ and $d_0(12)$ as unknown parameters by assuming $a(12) = a(16)$ and $d_0(16) - d_0(12) = 160$ pm. The fitting was much better than the first one and the determined parameters were as follows: $a(12) = 18.5$ and $d_0(12) = 215$ pm. Here, the fitting treating both $a(12)$ and $a(16)$ as different unknown parameters gave little improvement. The value of 215 pm seems to be a little larger than the d_0 estimated geometrically but both the values of $a(12)$ and $d_0(12)$ were quite reasonable compared with the respective values of the Ar-β-quinol clathrate determined from far-infrared spectra [24] ($a = 23.2$ and $d_0 = 236$ pm).

Heat capacity curves of $(2/3)C(12)$ and $(1/3)C(16)$ calculated with the parameters determined by the second fitting are shown in Fig. 6 by lines C and D, respectively. $C(16)$ has a larger heat capacity than $C(12)$ in the low temperature region. This arises from the fact that $d_0(16)$ is 160 pm larger than $d_0(12)$; i.e., the larger the d_0 value, the narrower the space between energy levels for the rattling as shown in eq. (3). It is revealed that the reason why the heat capacity of argon in the hydrate cage is larger than that in the β-quinol clathrate at low temperatures is due to the contribution of argon in the larger 16-hedral hydrate cages (375 pm from the fitting).

As described above, the heat capacity of argon in the hydrate cages could be analyzed well by using the one-dimensional Pöschl-Teller potential. This, though indirectly, gives evidence for the validity of the underlying assumptions: the additivity of the heat capacities of the guest and host and representing the heat capacity of the host lattice by that of hexagonal ice.

4. Conclusion

The results on the proton-ordering in the host hydrogen-bonded system in both pure and KOH-doped Ar-hydrates are quite different from those in pure and KOH-doped THF-hydrates. This indicates that the guest molecules affect to some extent the thermodynamic properties of proton-ordering in the host. Argon should make a much smaller interaction with the hydrogen-bonded system than the THF-molecule so that the results on proton-ordering obtained in the Ar-hydrate would be close to the properties of the hypothetical empty host lattice. This is supported by the fact that the additivity of heat capacities of the guest and host is valid in the Ar-hydrate. It is interesting to consider what properties of the guest can affect the hydrogen bonded system. It is plausible to infer that the dipole moment of the guest molecule induces a local electric field in the cage and changes the stability of some local structures of the hydrogen-bonded system. Furthermore, the oxygen atom in ether or ketone molecules like THF has a possibility to form a transient hydrogen-bond with the host lattice. We have measured only two hydrate systems so far; one has the smallest spherical guest possible and the other has a large dipolar one. The clathrate hydrates of larger nonpolar species (Kr, SF_6, 1,4-dioxane), molecules having different dipole moments (acetone, cyclobutanone, etc.), and those also forming the structure I hydrate as well (Xe, ethylene oxide, etc.) will be measured in order to provide some answers to the above problems.

Acknowledgement

This work was supported partly by a Grant-in-Aid for Scientific Research No. 57430002 from the Ministry of Education, Science and Culture, and partly by the Takeda Science Foundation.

References

1. D. W. Davidson, Y. P. Handa, C. I. Ratcliffe, J. S. Tse, and B. M. Powell: *Nature* **311**, 142 (1984).
2. M. von Stackelberg and H. R. Muller: *Naturwiss.* **38**, 456 (1951).
3. T. C. W. Mak and R. K. McMullan: *J. Chem. Phys.* **42**, 2732 (1965).
4. R. M. Barrer and A. V. J. Edge: *Proc. Roy. Soc., Ser. A* **300**, 1 (1967).
5. D. R. Marshall, S. Saito, and R. Kobayashi: *AIChE J.* **10**, 202, 723 (1964).
6. S. R. Gough, E. Whalley, and D. W. Davidson: *Can. J. Chem.* **46**, 1673 (1968).

7. O. Yamamuro, M. Oguni, T. Matsuo, and H. Suga: *Bull. Chem. Soc. Jpn.* **60**, 1269 (1987).
8. N. H. Fletcher: *The Chemical Physics of Ice*, Cambridge Univ. Press (1970).
9. M. Oguni, N. Okamoto, O. Yamamuro, T. Matsuo, and H. Suga: *Thermochim. Acta* **121**, 323 (1987).
10. O. Yamamuro, M. Oguni, T. Matsuo, and H. Suga: *Solid State Commun.* **62**, 289 (1987).
11. O. Yamamuro, M. Oguni, T. Matsuo, and H. Suga: *J. Phys. Chem. Solids*, in press.
12. R. E. Hawkins and D. W. Davidson: *J. Phys. Chem.* **70**, 1889 (1966).
13. Y. Tajima, T. Matsuo, and H. Suga: *Nature* **299**, 810 (1982).
14. Y. Tajima, T. Matsuo, and H. Suga: *J. Phys. Chem. Solids* **45**, 1135 (1984).
15. O. Yamamuro, M. Oguni, T. Matsuo, and H. Suga: *J. Phys. Chem. Solids* **48**, 935 (1987).
16. N. G. Parsonage and L. A. K. Staveley: *Disorder in Crystals*, Chap. 11, Clarendon Press, Oxford (1978).
17. Y. P. Handa: *J. Chem. Thermodyn.* **18**, 891 (1986).
18. Y. P. Handa and J. S. Tse: *J. Phys. Chem.* **90**, 5917 (1986).
19. A. C. H. Hallett: *Argon, Helium, and the Rare Gases*, Vol. 1, Chap. IX, Ed. G. A. Cook, Interscience Publications, New York – London (1961).
20. J. H. van der Waals: *Trans. Faraday Soc.* **52**, 184 (1956).
21. H. Suga and S. Seki: *J. Non-cryst. Solids* **16**, 171 (1974).
22. O. Haida, T. Matsuo, H. Suga, and S. Seki: *J. Chem. Thermodyn.* **6**, 815 (1974).
23. G. A. Neece and J. C. Poirier: *J. Chem. Phys.* **43**, 4282 (1965).
24. J. C. Burgiel, H. Meyer, and P. L. Richards: *J. Chem. Phys.* **43**, 4291 (1965).